Carbon 138 (2018) 134–142

Contents lists available at ScienceDirect

Carbon

journal homepage: www.elsevier.com/locate/carbon

Strength loss of carbon nanotube fibers explained in a three-level hierarchical model

Enlai Gao [a], Weibang Lu [b], Zhiping Xu [a, c, *]

[a] Applied Mechanics Laboratory, Department of Engineering Mechanics and Center for Nano and Micro Mechanics, Tsinghua University, Beijing 100084 China
[b] Division of Advanced Materials & Innovation Center for Advanced Nanocomposites, Suzhou Institute of Nano-Tech and Nano-Bionics, Chinese Academy of Sciences, Suzhou 215123, China
[c] Applied Mechanics and Structure Safety Key Laboratory of Sichuan Province, School of Mechanics and Engineering, Southwest Jiaotong University, Chengdu 611756, China

ARTICLE INFO

Article history:
Received 12 February 2018
Received in revised form
22 May 2018
Accepted 25 May 2018
Available online 25 May 2018

ABSTRACT

Although the tensile strength of carbon nanotubes inherited from the sp^2 hexagonal carbon lattice is as high as 120 GPa, the state-of-the-art mechanical resistance of carbon nanotube fibers is below 10 GPa. Material imperfections embedded in the complex microstructures are responsible for this remarkable reduction across multiple length scales. In this study, we rationalize this multi-scale degradation of mechanical performance through theoretical analysis of the processing-microstructure-performance relationship for carbon nanotube fibers based on the experiment data, offering a simplified model that not only quantifies the breakdown of material strength at the nanotube, bundle, and fiber levels, respectively, but also provides practical advices to optimize the manufacturing processes for elevated mechanical performance.

© 2018 Elsevier Ltd. All rights reserved.

1. Introduction

Carbon nanotubes (CNTs), since the very first reports of their discovery, have been holding great promises in various applications by offering unsurpassable material stiffness (~1 TPa), strength (~120 GPa) and resilience (~15% strain to failure) [1,2]. A wide spectrum of proposals have been made from reinforcing composites to the only candidate that can be used to build space elevators with structural reliability [3]. However, after about 20 years of intensive work, the mechanical performance of CNT fibers, which are the macroscopic forms of nanoscale tubules, is still not competitive with commercial carbon fibers (Fig. 1) [4–6]. This disappointing fact is attributed to their unresolved microstructural complexity, including inherent lattice defects of CNTs, the disordered stacking and insufficient length (sub-millimeter) of CNTs in closely-packed bundles, as well as the wavy morphology and entangled topology of the bundle assembly [7–10]. Multiple types of characteristic structural units and their interactions determine the load transfer within the CNT fibers from the atomic scale to the macroscopic scale. Only recently there have been several studies elucidating the hierarchical microstructures of CNT fibers through advanced characterization techniques including electron microscopies, X-ray scattering, which provide not only illustrative views of the multi-level structural units and their interfaces, but also offer quantitative information about their dimensions that helps for constructing theoretical models to characterize their mechanical behaviors [11–13]. Furthermore, the studies by *in-situ* Raman spectroscopy elucidate the multi-level mechanism of material deformation and microstructural evolution in CNT fibers under stretching, from elastic elongation, strengthening to damage and failure [14,15]. Depth-profiled polarized Raman spectroscopy data shows that twisting cannot be fully transferred through the whole CNT fiber and nanotubes within a fiber align non-uniformly in the radial direction [16]. Rate-dependent failure mechanisms were also elucidated for the CNT fibers, with inter-tube slippage occurring at low rates while cascade-like breaking processes dominate at high rates due to the misalignment of CNTs [17–19].

Unlike carbon fibers that are synthesized from polymeric precursors through high-temperature treatments including oxidation and carbonization [52], CNT fibers are assembled from individual

* Corresponding author. Applied Mechanics Laboratory, Department of Engineering Mechanics and Center for Nano and Micro Mechanics, Tsinghua University, Beijing 100084 China.
E-mail address: xuzp@tsinghua.edu.cn (Z. Xu).

https://doi.org/10.1016/j.carbon.2018.05.052
0008-6223/© 2018 Elsevier Ltd. All rights reserved.

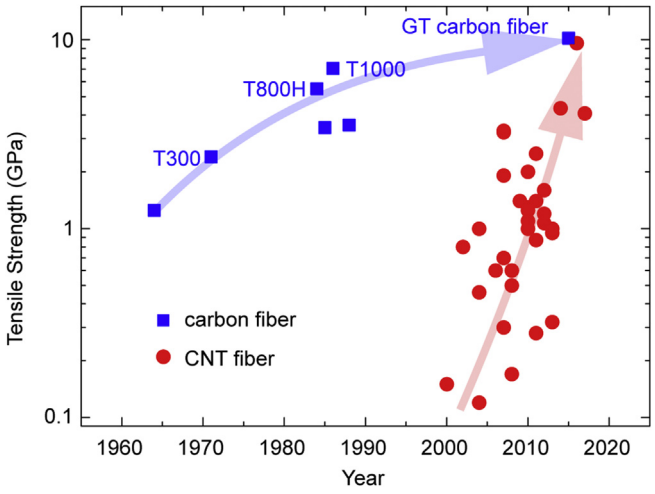

Fig. 1. Evolution of the tensile strength of CNT fibers and carbon fibers. The data are collected in Table S1 [10,11,17,20–50] and Table S2 [51,52]. (A colour version of this figure can be viewed online.)

CNTs through weak inter-tube interaction, assisted by mechanical driving forces during, for example, dry or wet spinning processes with much lower energy and economic costs [40,42]. This bottom-up procedure naturally spans over multiple length scales through forming bundles from individual CNTs, and then forming fibers from wavy and entangled bundles [53]. Normally, CNTs produced from the chemical vapor deposition (CVD) processes inevitably contain some defects that reduces their mechanical strength [9,54–58]. Meanwhile, the CNTs feature limited lengths, usually on the order of a few micrometers to millimeters. The interface between CNTs has high cohesive strength but low shear strength [59]. In consequence, CNTs preferably form locally closely-packed bundles and exhibit a certain stacking order during CNT growth and the processing of individual CNTs into assemblies [12,60]. Finally, the as-spun and processed CNT fibers are consider as a complex network with CNT bundles branching out (forking) and merging in Refs. [12,61], which is reminiscent of the highway network with branches and hubs. Although it is difficult to determine the bundle length directly from the SEM images as there is no bundle termination characterized (Fig. 2c), one would expect the value to be much larger than the length of individual CNTs and the inter-hub spacing along the fiber axis.

In this work, we break down the microstructural complexity of CNT fibers into three levels, that are the primary (individual CNTs), secondary (bundles with closely-packed CNTs) and tertiary (the fiber as an assembly of the bundles) levels, and developed theoretical models to characterize the reduction in the tensile strength across these levels (Fig. 2). Considering the advances in the control of CNT growth with high quality and yield, as well as efficient fiber spinning and post-processing techniques, the multi-scale analysis could quantify the loss of mechanical properties within each process, and offer practical suggestions for rational optimization of the manufacturing process toward CNT fibers with elevated mechanical performance.

2. Theory

The strength of individual CNTs, CNT bundles and fibers has been studied intensively. In the CNT level, both experimental [64–66] and molecular simulation [67] studies show that the cumulative distribution function of failure probability for a CNT with length l can be well modeled using a two-parameter Weibull distribution function $F(\sigma) = 1 - \exp[-(\sigma/\sigma_l)^m]$, where m is a shape parameter that depends on the type and density of defects in samples, that is, the 'Weibull modulus', and σ_l is a scale parameter, indicating the statistical nature of tensile strength (Fig. 2g). In the bundle level, the pathway of force transmission through the bundle consists of both the CNTs themselves and their interfaces [68]. Load transfer across the interfaces limits the overall performance of bundles if these interfacial contact area between neighboring tubes is not large enough, by considering the insufficient length of CNTs and low shear strength between CNTs. The up-scaling of mechanical performance of the bundle could be captured in shear-lag models, which have been discussed by several groups [8,68–70]. In the fiber level, the load transfer between bundles can be also captured in shear-lag models under the assumption that the bundles in fiber have a certain length and stacking manner that is similar to that of the nanotubes in bundle, while the microstructural complexity of CNT fibers including the waviness, entanglement and non-ideal contact were not considered [7,15]. Simplified models including a two-scale damage mechanics model [71] and a two-level interfacial mechanical model [15] were proposed to explain and optimize the mechanical performance of CNT fibers. However, a model that directly quantify the strength loss from an individual CNT to the fiber in the characteristic length scales is still missing, which prohibit reliable assessment of the fiber performance and further improvement in the fiber strength by optimizing the fabrication processes.

In this work, a three-level model is developed. In the primary level (individual CNTs), a statistical strength model is used to link the tensile strength of the perfect CNT (σ_0) and that with defects (σ_1). In the secondary level considering bundles with closely-packed CNTs, a shear-lag model is used to predict the tensile strength of CNT bundles (σ_2) from σ_1 and the packing geometry. In the tertiary level, the fiber is considered as an assembly of the bundles, where a wavy model is developed to map the tensile strength of the CNT bundles (σ_2) to the fiber (σ_3).

In order to calculate the strength of CNTs, CNT bundles and fibers, their cross-section area has to be well defined. For CNTs, the strength is usually defined as the tensile force normalized by the cross-section area of load bearing shells $A_{CNT} = n\pi dt$ [64,72–74], where n is a factor defining the efficiency of load transfer into the graphitic shells, d is the diameter of the outermost CNT shell and $t = 0.34$ nm is the effective shell thickness defined as the interlayer distance of graphite. For multiwalled carbon nanotubes (MWNTs) that fail through the well-known 'sword-in-sheath' mode, only the outermost wall bears the load and $n = 1$, $A_{CNT} = \pi dt$ [64,72]. For bundles, the sum of load bearing cross-section area of CNT shells in the bundle is counted to calculate the bundle strength. The tensile strength of fiber is firstly calculated from the total load bearing cross-section area of CNT shells as σ_s. Considering that the shells bearing no load also make contribution to the mass and volume of the fiber, the specific strength of the fiber can then be written as $r\sigma_s/\rho_g$, where r is mass fraction of loading bearing CNT shells in the fiber, and $\rho_g = 2.25$ g/cm^3 is the mass density of graphite. Consequently, the nominal strength measured in experiments can be converted from σ_s as $\sigma_3 = r\sigma_s\rho_a/\rho_g$, where ρ_a is the mass density of CNT fiber.

3. Results

3.1. Strength reduction of individual CNTs with defects

CNTs synthesized from CVD, arc-discharge, laser ablation, or the high pressure carbon monoxide method inevitably contain inherent defects, such as vacancies and topological defects, which create stress localization. Collins estimated the concentration for

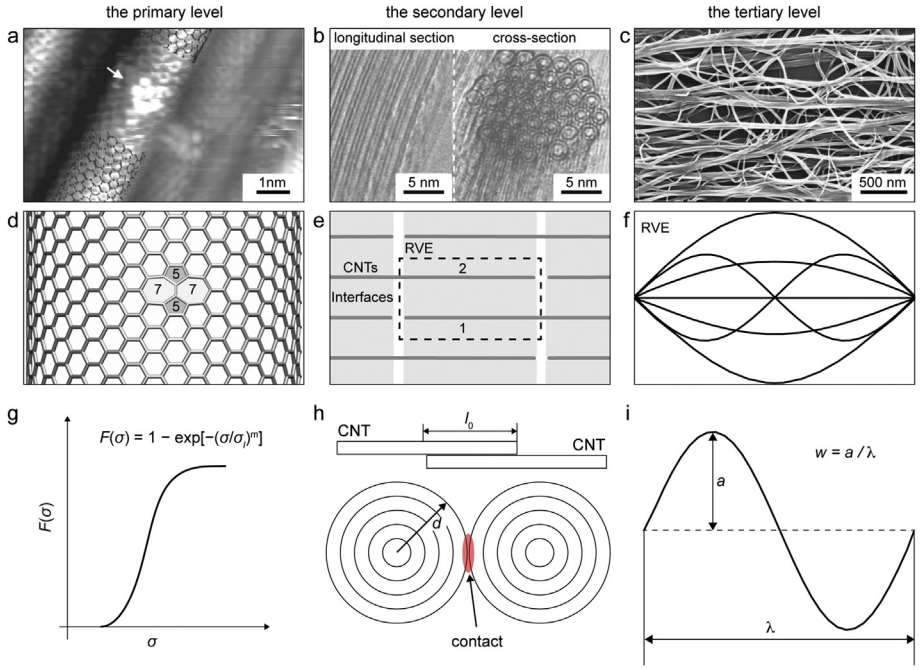

Fig. 2. Microstructures of a CNT fiber, broken down to a three-level hierarchy - individual CNTs, their closely-packed bundles and the wavy, entangled bundle network. Experimental characterization: (a) The scanning tunneling microscopy (STM) image of a SWNT containing topological defects [62]. (b) Longitudinal and cross-sectional tunneling electron microscopy (TEM) images of a DWNT bundle exhibiting a closely-packed structure in the hexagonal lattice [63]. (c) The SEM image of the macroscopic CNT assembly, where bundles branching out and merging in throughout the whole network, making an extended, inherently interconnected network. Abstraction in theoretical models: (d) A SWNT with a representative Stone-Wales (5-7-7-5) topological defect. (e) The representative volume element (RVE) of closely-packed CNT bundles where tensile load is transferred through stretching of the CNTs and shear through their interfaces. (f) A RVE of the bundle network, modeled by CNT bundles with non-uniform distribution of waviness. Illustration of the key model parameters: (g) Strength of the Weibull distribution. (h) Contact geometry between closely-packed CNTs in the bundle. (i) A wavy bundle with specific waviness *w*. (A colour version of this figure can be viewed online.)

common types of defects from their formation energies in CNTs, which set the lower bounds for the defect concentrations [57]. For example, considering the formation energy $E_f = 4$ eV of a di-vacancy defect in CVD-grown single-walled CNTs (SWNTs) with diameter $d = 1$ nm, the equilibrium separation between defects, which was predicted from thermodynamics through the Boltzmann factor $\exp(-E_f/k_BT)$, is ~50 μm even at 3000 K, while the value measured by the atomic force microscopy is only 350 nm for SWNTs produced by arc-discharge [55]. It is shown that using the heat of formation instead of E_f predicts higher defect concentration, which agrees better with the experimental observation [75]. For a CNT, experimental [64–66] and molecular simulation [67] studies show that the cumulative distribution function of failure probability for a CNT with length l can be well modeled using a two-parameter Weibull distribution function $F(\sigma) = 1 - \exp[-(\sigma/\sigma_l)^m]$ (Fig. 2g), where m is a shape parameter that depends on the type and density of defects in samples, that is, the 'Weibull modulus', and σ_l is a scale parameter, indicating the statistical nature of tensile strength. The tensile strength of defective CNTs with length of l can be derived as the mean value of the Weibull distribution, expressed in the Gamma function, $\sigma_1 = \sigma_l\Gamma(1 + 1/m)$, where $\sigma_l = \sigma_{l0}(l/l_0)^{-1/m}$, σ_{l0} is the scale parameter of Weibull distribution for CNT with length l_0. Hence, the effect of defects on the tensile strength of CNTs expresses a distinct length dependence or size effect, and the strength is reduced from that of a defect-free CNT (σ_0) to that of a defective CNT with length l (σ_1), that is

$$\sigma_1 = \alpha_1\sigma_0 \tag{1}$$

where α_1 is the primary reduction factor that characterizes the tensile strength reduction due to the presence of defects in the CNT with a certain length, which can be determined by $\alpha_1 = \sigma_1/\sigma_0$ or $\alpha_1 = \frac{\sigma_{l_0}}{\sigma_0}\left(\frac{l}{l_0}\right)^{-\frac{1}{m}}\Gamma\left(1+\frac{1}{m}\right)$. As the experimental determination of defect concentration in CNTs remains as a challenge, we make quantitative estimation here based on the statistical strength model. The diameter of CNTs mostly ranges from 1 to 2 nm for SWNTs, 2–10 nm for double-walled carbon nanotubes (DWNTs), and 10–50 nm for MWNTs, and the lengths are typically in the range of ~500, 700–1000 and 100–6000 μm, respectively (Table S3) [6]. Molecular dynamics (MD) studies show that the presence of low-concentration (on the order of 1%) topological defects or vacancies in SWNTs remarkably reduces their tensile strength from over 100 GPa to below 50 GPa as the length of CNT exceeds dozens of micrometers (Fig. 3) [67]. Specifically, as the length of a SWNT increases from 0.01 to 10 μm, the tensile strength is reduced from 138 to 56.1 GPa and 108 to 49.5 GPa with the presence of 2% topological defects and 1.5% vacancy defects, respectively. The presence of statistical size effect makes long CNTs weak, which can explain the difference between the low strength of micrometer-long samples of CNTs measured from experimental tests – SWNTs (13–52 GPa, 30 GPa in average) [76], DWNTs (17–43 GPa, 21 GPa in average) [72], tri-walled carbon nanotubes (TWNTs, 13–46 GPa, 23 GPa in average) [72], and MWNTs (11–63 GPa, 28 GPa on average [64], 10–66 GPa, 24 GPa in average [73]), and the high value (100–180 GPa) theoretically predicted for defect-free CNTs (Fig. 3) [1,2]. In addition, it should be noted that the length dependence could be weakened with an increased Weibull shape parameter by reducing the defect concentration (Fig. 3) [67,77]. These results clearly indicate that the length and defect (type and concentration) of individual CNTs are the key factors limiting the tensile strength of individual CNTs.

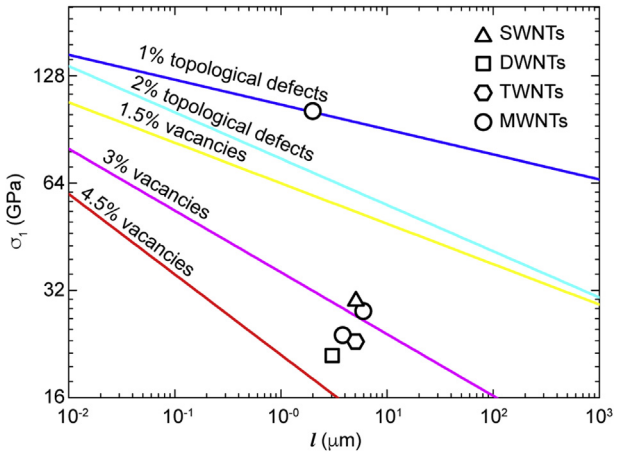

Fig. 3. Molecular simulation results (the lines) of the statistical strength reduction for a SWNTs with various concentration of topological defects or vacancies [67] that are fitted by assuming $\sigma_0 = 120$ GPa, compared with the measured tensile strength for SWNTs [76], DWNTs [72], TWNTs [72] and MWNTs [73,74] by experiments (the symbols) with reductions from the intrinsic defects. (The parameters are listed in Tables S5 and S6). (A colour version of this figure can be viewed online.)

3.2. Strength of bundles composed of finite-length CNTs

The atomistically smooth, non-polar graphitic walls with an interlayer binding energy of ~0.3 J/m^2 endow CNTs high cohesive strength while low shear strength [59]. As a result, during the growth of CNTs and the processing of individual CNTs into assemblies, CNTs preferably form locally closely-packed bundles [12,60]. Experimental data suggests that typical diameters of SWNT, DWNT and MWNT bundles are 19–41, 11–28 and 10–100 nm, consisting of 91–444, 14–91, and ~25 individual CNTs, respectively [12,76,78] (Table S4). However, determination of the bundle length is technically challenging because of their ultrahigh aspect ratio. Considering the finite length of CNTs, the tensile strength of a bundle is determined by the trade-off between the tensile performance of CNT walls as well as the load transfer among the CNTs through the interfaces, as captured by the model with stacked shear-lag units (Fig. 2e). Here we consider a bundle consisting of closely-packed identical CNTs with reduced strength by defects, and then apply the tension-shear (TS) model to predict the overall mechanical performance with explicit dependence on microstructural parameters such as the length of CNTs and the staggering order quantified through the overlap between CNTs [8,68,69]. The thickness or diameter dependence is not considered here as the number of CNTs in a bundle, on the order of 10–100, is relatively large [12,76,78]. In addition, it should be noted that, this statistical size effect (length, diameter of the CNTs) applies for the bundles as well, which, however, can also be neglected by considering the fact that shear-lag units consist of CNTs, forming the so-called 'Daniels' bundle' [79], and a large number of parallel units in the cross-section suppresses the size effect (see notes in the **SI** and Fig. S1) [80]. We first explore the effect of stacking orders on the bundle strength [68,81] by considering a regularly half-staggered bundle with uniform overlap length of $l/2$ between the CNTs. Here l is the length of CNTs. This bundle fails in two distinct modes, that are, fracture of the CNTs (denoted as mode T), or inter-tube sliding among neighboring CNTs (mode I). The selection of failure modes is determined by the geometries and mechanical properties of CNTs and their interfaces, and the strength is $\sigma_2 = \sigma_1 A_{CNT}/2A_{CNT} = \sigma_1/2$ for mode T, and $\tau_s \beta A/2A_{CNT}$ for mode I, considering that only 50% CNT in the weakest cross-section bears the peak force (Fig. 2e). Here τ_s is the interfacial shear strength among CNTs, and $A = \pi d l_o$ is the total surface area of a CNT in contact with its neighbors with overlap length l_o ($l_o = l/2$ for regularly half-staggered bundles). The contact between cylindrical CNTs is only part of their surfaces, denoted as βA with a parameter β. Notably, large-diameter CNTs could collapse into 'dog-bone' shapes with large values of β, as driven by the inter-wall van der Waals attraction [82]. Considering the balance between load bearing through the CNTs and that across their interface ($\sigma_1/2 = \tau_s \beta A/2A_{CNT}$), a critical overlap length l_c can be derived from as $l_c = n\sigma_1 t/\beta\tau_s$, beyond which the interfacial load transfer is sufficient to proceed with mode-T failure. In addition σ_1, τ_s and β are the two key factors to determine l_c. The shear strength τ_s was measured as 0.08–0.30 MPa for MWNTs, which depends on the matching of lattice registries among neighboring CNTs that is technically difficult to be determined [83]. This value is close to the interlayer shear resistance in high-quality natural crystalline graphite, 0.25–0.75 MPa with a mean value of 0.48 MPa [84], which has been widely adopted in the literature [83,85,86]. In addition, the value of β can be expected to vary with the contact geometry from touching round tubes to stacks of flattened 'dog bone' CNTs (see Fig. 4a–c for cylindrical [87], partially-collapsed [88], and fully-collapsed CNTs [82]). The value of l_c is thus estimated to be ~10–10^3 μm, from typical values of σ_1 (~30 GPa), n (1), β (10%–100%) and τ_s (0.1 MPa–1 MPa) (Fig. 4d), and we can rewrite σ_2 as $\sigma_1 l/4l_c$ for $l < 2l_c$, and $\sigma_1/2$ for $l \geq 2l_c$. In practice, the stacking order in a CNT bundle appears to be randomly staggered for wet-spun or dry-spun fibers [12,40], which reduces the overall strength of the bundles due to the insufficient load transfer [68,81]. By assuming that l_o is uniformly distributed between 0 to l, the average tensile strength can be derived as the average value, that is $\sigma_2 = l\sigma_1/8l_c$ for $l < 2l_c$ and $(l - l_c)\sigma_1/2l$ for $l \geq 2l_c$. As a result, the tensile strength of a CNT bundle (σ_2) can be written as

$$\sigma_2 = \alpha_2\sigma_1 = \left(\frac{l}{4l_c}\right)\sigma_1 \text{ for } l < 2l_c \text{ or } \frac{\sigma_1}{2} \text{ for } l > 2l_c \quad (\text{for half} - \text{staggered bundles}) \tag{2a}$$

$$= \left(\frac{l}{8l_c}\right)\sigma_1 \text{ for } l < 2l_c \text{ or } \left(\frac{l - l_c}{2l}\right)\sigma_1 \text{ for } l > 2l_c \quad (\text{for randomly} - \text{staggered bundles}) \tag{2b}$$

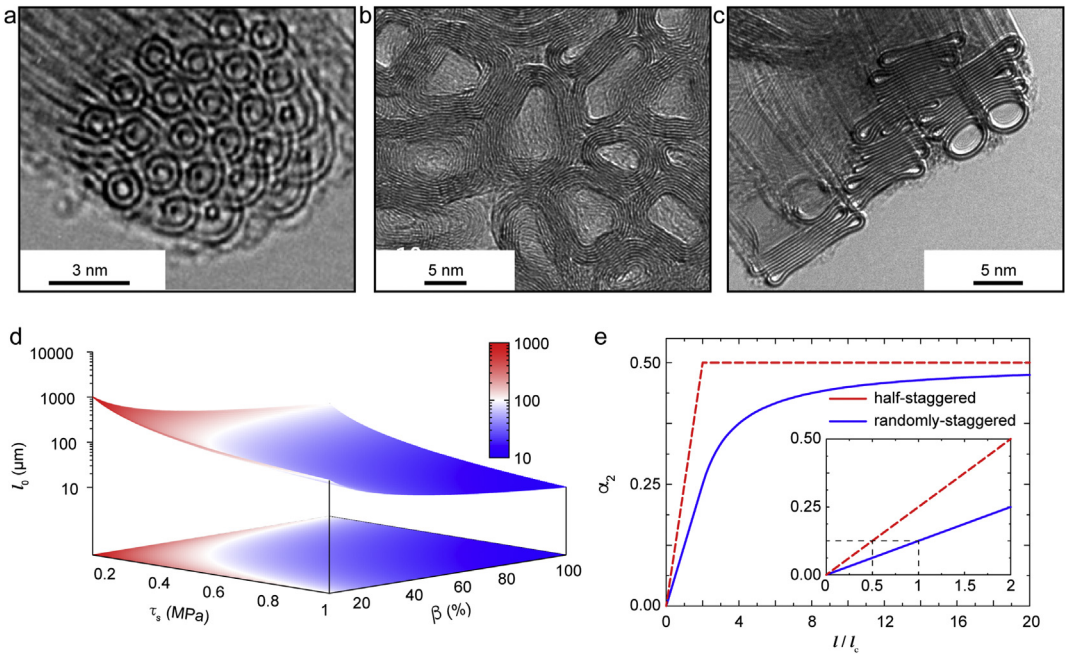

Fig. 4. The strength reduction in a CNT bundle due to insufficient load transfer between the closely-packed CNTs. (a) High-resolution cross-sectional TEM images of the nearly perfect cylindrical DWNTs [87], (b) partially-collapsed MWNTs [88], (c) and fully-collapsed DWNTs with diameter greater than 5 nm (Note that there are also non-collapsed tubes at the edge of the bundle) [82]. (d) The critical overlap length between CNTs in the bundles where the intra-tube and inter-tube load transfer is balanced, plotted as a function of the interfacial shear strength and effective contact factor. (e) The reduction factor α_2 plotted as a function of the overlap length, for the half-staggered and randomly-staggered bundles. (A colour version of this figure can be viewed online.)

where α_2 is the secondary reduction factor characterizing the tensile strength reduction from defective CNT to closely-packed bundles. For half-staggered and random-staggered CNT bundles, the value of α_2 depends on l/l_c, where l_c is the function of the interfacial contact area and shear strength (Fig. 4d). The upper bound of the tensile strength can thus be estimated as 50% on condition that the load transfer among the CNTs in the bundle is sufficient (Fig. 4e). The critical length of CNTs for saturation in the tensile strength of a bundle is much larger for random-staggered CNT bundle (~$20l_c$) than that for half-staggered CNT bundle ($2l_c$), as shown in Fig. 4e. In practice, the *in-situ* Raman spectroscopy based study of CNT fibers under tensile loading reveals that the individual CNTs deform elastically without visible damage, and the fracture of fibers is attributed to the slippage among CNTs or in the mode I [14]. These results clearly indicate that the interfacial shear strength and contact among CNTs are the key factors limiting the tensile strength of CNT bundles.

3.3. Load transfer in fibers with network microstructures

CNT fibers fabricated from wet-spun, dry-spun or floating-CVD techniques feature continuous and interlocked network microstructures where bundles branch out (bundling forking) and merge in, in reminiscence of the highway network with branches and hubs [12,53,61]. There are no distinct termination of the bundles over the field of view in the SEM images (Fig. 2c), making it impossible to measure the bundle length. Moreover, the bundles are usually not straight between the hubs, but rather display a

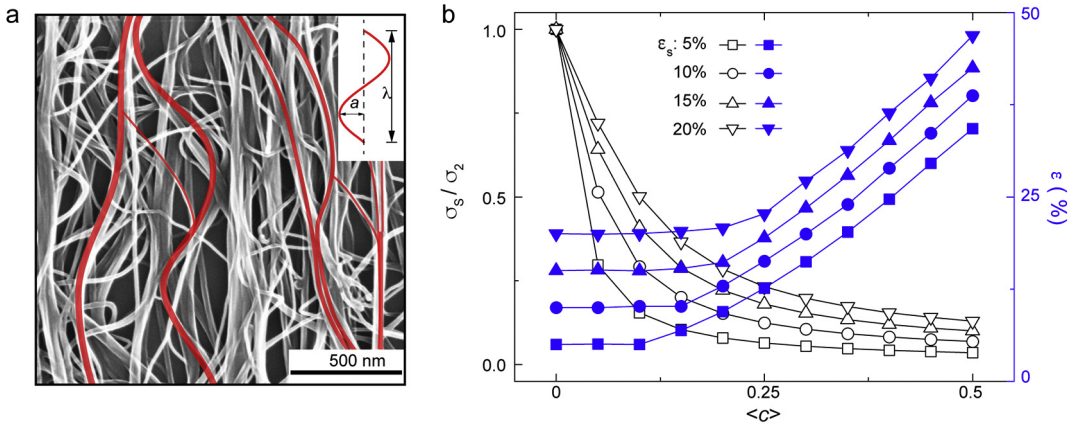

Fig. 5. The strength reduction resulted from the misalignment and porosity in the entangled CNT bundle networks of a CNT fiber. (a) The SEM images and schematic illustration of wavy CNT bundles in the CNT network. (b) The tensile strength and strain to failure of a CNT network consisting of bundles with different strain to failure and mean curl ratios. (A colour version of this figure can be viewed online.)

certain degree of curl or waviness along their profiles (Fig. 5a). This wavy morphology can be attributed to their very large aspect ratios and notable forced distortion in the fabrication processes [12]. The hierarchical microstructure of macroscopic CNT assemblies was mapped with quantitative measured through electron microscopies and X-ray scattering experiments [13]. The interface between the bundles is critical in defining the load bearing capacity of the fibers (Fig. S2). For bundles in contact with strong interfaces or those with large overlap area that allow sufficient load transfer efficiency, the bundle will be stretched till break (Fig. S2a), while weak interfaces between the bundles will fail by sliding (Fig. S2b), endowing additional mechanical resistance of the fiber. Considering that the contribution of interfacial sliding between bundles to the fiber strength is negligible, one could simplify the load transfer path in the bundle network by considering the stretching of load-bearing bundle chains only (Figs. S2a and S2c). From the scanning electron microscopy (SEM) images, the network microstructures of CNT fibers can be rationalized into an assembly of successive CNT bundle with finite waviness (Fig. S3a). The waviness of a bundle can be quantified via the factor $w = a/\lambda$, where λ is the characteristic wavelength and a is the amplitude. The curl ratio c is defined as $l_b/s - 1$, where l_b is the contour length of the bundle and s is its end-to-end distance [89–92], and the relation between w and c is $c = 2\int_0^{1/2}\sqrt{1+2\pi w\cos^2(2\pi x)}\,dx - 1$. To replicate the curling nature of CNT bundles in the fiber samples, a truncated normal distribution of curl ratio $f(c)$ can be used, that is, $f(c) = \frac{2}{\chi\sqrt{2\pi}}\exp\left(-\frac{c^2}{2\sigma^2}\right)$ for $c \geq 0$ and $f = 0$ otherwise. Here χ is the standard deviation of the distribution. In this wavy model, following assumptions are made: (1) the bundle network is divided into hub and branch. In the hub segment, load transfer between the bundles is sufficient, and thus the hub can be treated as a thicker bundle, while in the branches, interaction between bundles are negligible. (2) The deformation of bundle network for a CNT fiber is affine, and can be captured by RVEs containing wavy bundles. (3) The mechanical resistance of a bundle is zero before straightened, and then exhibits a linearly elastic behavior before it fails, that is to say, the bending resistance of the bundle is omitted considering the very high aspect ratios. When the nominal strain ε is applied to the bundle network, the tensile stress $\sigma(\varepsilon, c)$ in each bundle with a specific value of c can be calculated as $\sigma(\varepsilon, c) = 0$ ($\varepsilon_a < 0$), $\varepsilon_a\sigma_2/\varepsilon_s$ ($0 \leq \varepsilon_a < \varepsilon_s$) or 0 ($\varepsilon_a \geq \varepsilon_s$), where $\varepsilon_a = (\varepsilon + 1)/(c + 1) - 1$ is the actual tensile strain that the bundle bears, and ε_s is the strain to failure of the bundle. The average value of c considering the randomness of curl ratio is $<c> = \int_0^\infty f(c)c\,dc = 2\chi/\sqrt{2\pi}$, the tensile stress of a CNT fiber under tensile strain ε is $<\sigma> = \int_0^\infty \sigma(\varepsilon, c)f(c)\,dc$, and the tensile strength σ_s can be extracted from the yield point in the strain-stress curve (Fig. 5 and Fig. S3). In practice, the wavy morphology of vertically aligned CNT samples is controlled by the growth condition (Fig. S3a), and can be further modulated through post-treatment [89,90,92]. For example, the curl ratio and waviness decrease from $c = 0.5$, $w = 0.25$ for the as-prepared samples to $c = 0.06$, $w = 0.08$, as the samples are densified [89,92]. Combining the theoretical model and experimental measurements, we evaluate the strength of CNT fibers with c ranging from 0 (straight) to 0.5 (extremely curly). The results show that the curl of bundles in CNT fiber remarkably reduces σ_s (Fig. 5b), and it also demonstrates that the tensile stress-strain behavior changes from brittle to ductile as c increases (Fig. S3b). The strain to failure ε_s is one of the most important parameters fed into the wavy model to calculate the fiber strength. With ε_s changing from 5%, 10%, 15%, to 20%, considering the diversity in the stacking order and length of CNTs in the bundle [68,76,78], tensile strength and strain to failure of the fibers change accordingly (Fig. 5b). The bundles with larger strain to failure values endow the fibers higher tensile strength and curl tolerance. This result also indicates the potential effects of the variation in the strain to failure of CNT bundles.

As the CNT shells bearing no load are counted for the mass, the specific strength of the fiber can be written as $r\sigma_s/\rho_g$, where r is mass fraction of loading-bearing shells in the fiber, and $\rho_g = 2.25$ g/cm^3 is the mass density of graphite. For comparison with experimentally measured strength values in literature, the nominal strength is calculated as $\sigma_3 = r\sigma_s\rho_a/\rho_g$, where ρ_a is mass density of the CNT fiber, and the value of σ_3 is related to the tensile strength of the closely-packed bundle (σ_2) as

$$\sigma_3 = \alpha_3\sigma_2 \tag{3}$$

where α_3 is the tertiary reduction factor that is determined by the wavy/curling nature of bundles and the porosity of CNT fibers. Unlike the primary and secondary reduction factors, the tertiary reduction factor cannot be explicitly expressed. However, it can be determined from experimental measurements of the waviness and density of CNT fibers following our theoretical protocol. Recent experimental studies show that CNTs in macroscopic assemblies can be straightened and aligned along the winding direction in the floating-CVD process at fast winding rates [11]. The randomly-, slightly- and well-aligned CNT film samples thus fabricated feature tensile strength of 0.277, 0.566, to 2.8 GPa. This study further shows that by increasing the packing density by rolling, the density could be improved from 0.53 to 1.85 g cm^{-3} that is close to that of the high-performance commercial carbon fibers, and the strength increases further from 2.8 GPa to 9.6 GPa. From the equation ($\sigma_3 = r\sigma_s\rho_a/\rho_g$) and changes in the strength and density, we find that $\sigma_3/\rho_a = r\sigma_s/\rho_g = 9.6$ GPa/1.85 g cm^{-3} $\approx$ 2.8 GPa/0.53 g cm^{-3}. Consequently, the effective load-bearing CNTs ($r\sigma_s/\rho_g$) may be intact that conforms to the fact that there is no significant damage of the CNT fibers after rolling treatment [11].

3.4. Strength reduction across multiple microstructural levels

Considering individual CNTs and bundles as the two basic structural units of CNT fibers, one could break down the reduction

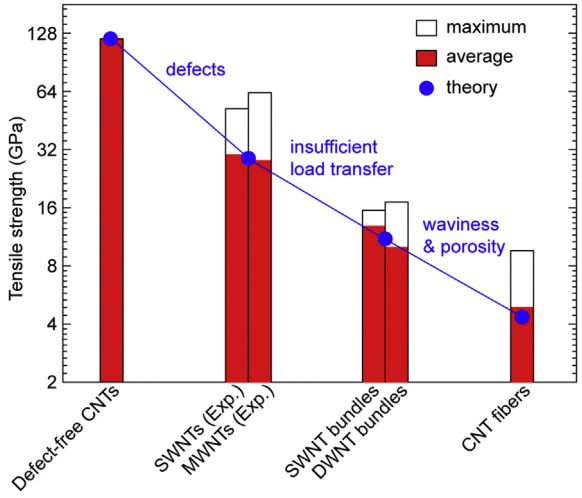

Fig. 6. The strength reduction from individual, defect-free CNTs to CNT fibers, broken down into a three-level hierarchy. The data is summarized in Table S7 [11,44,64,68,76,78,93]. (A colour version of this figure can be viewed online.)

of material strength into three separate mechanisms – the stress localization due to the presence of defects in CNTs (Fig. 2a and d), the insufficient load transfer among CNTs in the bundle (Fig. 2b and e), and the curly, porous network of bundles (Fig. 2c and f). With a typical length (~1000 μm) and defect concentration (1.5% vacancies) of the CNT, the strength is estimated to be reduced to 24.3% (α_1) of the ideal strength, from 120 GPa to 29.2 GPa (Eq. (1) and Fig. 3). For the bundles, further reduction of the strength depends on both the finite length of CNTs and their interaction (Eq. (2) and Fig. 4e). With a typical set of parameters ($l/l_c = 4$ for randomly-staggered bundles), one could estimate further reduction to 37.5% (α_2) of the CNT strength, that is $29.2 \times 37.5\% = 11.0$ GPa (Fig. 5b). In the next level of hierarchy, we model the bundle network as an assembly of the bundles with low-density, wavy morphology. Taking a typical parameter set ($r = 0.9$, $\rho_a = 1.5$ g/cm^3, $\rho_g = 2.25$ g/cm^3, $\varepsilon_s = \sim 15\%$ and $c = 0.05$), we find that the reduction at this network level is 38.5% (α_3) of the bundle strength, that is $11.0 \times 38.5\% = 4.2$ GPa (Eq. (3) and Fig. 5b). Combining these three steps of strength reduction, one finally reaches the conclusion that the ideal strength of a perfect CNT, 120 GPa, reduces to a much lower strength of a CNT fiber, ~4 GPa, which is comparable to the reported values for CNT fibers (Fig. 1). In addition, these three reduction factors estimated from theoretical models show excellent agreement with the trends of strength reduction characterized experimentally, from the nanotubes, bundles to the fibers (Fig. 6). Although these estimated values quantitatively depend on the structural parameters we chose, one could reasonably simplify the complex processing-microstructure-properties relationship into a phenomenological formalism

$$\sigma_3 = \alpha_3\alpha_2\alpha_1\sigma_0 \tag{4}$$

where these three reduction factors can be closely related to the processing conditions of CNT synthesis and fiber fabrication.

4. Discussion

4.1. Suggestions for the design of fiber fabrication processes

Considering the microstructural complexity and hierarchy of CNT fibers, it is not practical to develop a quantitative multi-scale model that bridges the gap between the CNTs and macroscopic fibers, and solve it mathematically. To guide the design and fabrication of high-strength CNT fibers, however, it would be more preferable to extract a few key parameters that capture the microstructures of fibers and relate them to the fabrication process, which could be correlated to the factors of strength reduction, $\alpha_{1\text{-}3}$, through our three-level model. The optimization of CNT growth conditions, the assembly of them into bundles, the final aligning and densification procedure, for example by stretching, winding, rolling and twisting, are thus closely related. Practically speaking, the alignment and densification processes are utilized in recent studies [11,37], while the other two steps are not well controlled. The elimination of defects during CNT growth is limited by thermodynamics, and the bundling processes cannot be well controlled for efficient load transfer among the CNTs.

Quantitative discussions on the mechanical performance of CNT fibers could then be made based on the formula we have. For example, by assuming that the CNT bundles are well aligned and closely packed ($\alpha_3 = 100\%$) in a fiber while the defects in CNTs and the insufficient load transfer among CNTs are still present ($\alpha_1 = 24.3\%$ and $\alpha_2 = 37.5\%$), the strength is estimated to be $\sigma_3 = \alpha_3\alpha_2\alpha_1\sigma_0 = 100\% \times 37.5\% \times 24.3\% \times 120$ GPa $= 10.9$ GPa. If very long and defect-free CNTs could be synthesized that span over the whole fiber ($\alpha_1 = 100\%$ and $\alpha_2 = 100\%$) [94] while the wavy nature of bundle network is preserved ($\alpha_3 = 38.5\%$), the strength of CNT fibers could reach $\sigma_3 = 38.5\% \times 100\% \times 100\% \times 120$ GPa $= 46.2$ GPa, although the defect control during growth is still limited. The strength of CNT bundles approaches that of individual CNTs as the finite-length effect is absent or negligible. Recently Bai et al. fabricated CNT bundles with ultra-long CNTs that span over the whole bundles, and the tensile strength was reported to be over 80 GPa [95]. Consequently, to assess the relevant applications with CNT fibers as the mechanical components, a reasonable target strength could be over 10 GPa.

4.2. Additional remarks

Although our discussion in this work is focused on the tensile strength of CNT fibers, the fiber stiffness can also be discussed in the same framework. Compared to the strength reduction, the defect has minor effects on the stiffness at low concentration. However, the saturation of bundle stiffness occurs at a much larger overlap length among the CNTs. That is to say, longer CNTs are needed for high stiffness, which is similar to the conclusion that high-modulus carbon fibers have larger crystalline graphite blocks than the high-strength fibers [96]. Furthermore, from bundle to assemblies, waviness significantly reduces the effective modulus of CNT assemblies as shown in previous studies [89,90].

Our study is limited as the load transfer mechanisms in the three microstructural levels are discussed separately, which are, however, coupled in practice. For example, tuning the interfacial interaction between individual CNTs or CNT bundles by creating crosslinks between surface functional groups inevitably reduces the mechanical resistance of the CNTs or bundles. The staggering and alignment of CNTs in bundles are also correlated to the size and geometry of bundles since they are determined during the same fabrication process. These facts could be discussed by generalizing the theory presented in this work.

5. Conclusion

In summary, a three-level model was proposed to understand load transfer in CNT fibers and the strength loss compared to defect-free CNTs, which was explained by mechanisms including stress localization due to the presence of defects in individual CNTs, insufficient load transfer in closely-packed bundle, and the porous, misaligned bundles in the fibers. By taking typical microstructural parameters characterized in recent experimental studies, we predict reasonable values of the fiber strength compared to the measured ones, which thus validate our simple model that can be used for the design of optimized fiber fabrication processes. This study also calls for more quantitative experimental work to characterize the microstructural features as abstracted in our theoretical model, which could further deepen our knowledge about the microstructural complexity of CNT fibers and its connection to macroscopic mechanical performance.

Acknowledgements

This work was supported by the Science Challenge Project through Grant No. TZ2018007, the Opening Project of Applied Mechanics and Structure Safety Key Laboratory of Sichuan Province through Grant SZDKF-1601, the National Key Research and Development Program of China (No. 2016YFA0203301), and the National Natural Science Foundation of China through Grant 11472150. The computation was performed on the Explorer 100 cluster system of Tsinghua National Laboratory for Information Science and Technology.

Appendix 1. A list of key parameters used in the theoretical analysis.

The primary level (Weibull) model	
α_1	the primary reduction factor
σ_0	tensile strength of a defect-free CNT
σ_1	tensile strength of a defective CNT
F	the probability of failure
l	length of a CNT
σ_l (σ_{l0})	the Weibull scale parameter for CNT with length l (l_0)
m	the Weibull shape parameter or Weibull modulus
σ	the mean value of tensile strength from the Weibull distribution
The secondary level (shear-lag) model	
α_2	the secondary reduction factor
σ_2	tensile strength of a CNT bundle
ε_s	strain to failure of a CNT bundle
d	diameter of a CNT
n	the scaling factor $A_{CNT}/\pi dt$
l_o	the overlap length of CNTs in a bundle
l_c	the critical overlap length for inter-tube load transfer
A_{CNT}	the load bearing cross-section area of a CNT
A	the total surface area of a CNT with the overlap length l_o
τ_s	interfacial shear strength between CNTs
β	the fraction of CNT surface area in contact with the neighbors
The tertiary level (wavy) model	
α_3	the tertiary reduction factor
σ_3	tensile strength of the CNT fiber
w	the waviness of a bundle
c	the curl ratio of a bundle
l_b	the contour length of a bundle
s	the end-to-end distance of a bundle
ρ_g	theoretical mass density of graphite
ρ_a	mass density of CNT fiber
r	mass fraction of load-bearing CNT shells in the fiber

Appendix A. Supplementary data

Supplementary data related to this article can be found at https://doi.org/10.1016/j.carbon.2018.05.052.

References

[1] B.I. Yakobson, P. Avouris, Mechanical properties of carbon nanotubes, in: M.S. Dresselhaus, G. Dresselhaus, P. Avouris (Eds.), Carbon Nanotubes: Synthesis, Structure, Properties, and Applications, Springer, 2001, pp. 287–327.
[2] R.S. Ruoff, D. Qian, W.K. Liu, Mechanical properties of carbon nanotubes: theoretical predictions and experimental measurements, C. R. Phys. 4 (9) (2003) 993–1008.
[3] B.C. Edwards, Design and deployment of a space elevator, Acta Astronaut. 47 (10) (2000) 735–744.
[4] L. Liu, W. Ma, Z. Zhang, Macroscopic carbon nanotube assemblies: preparation, properties, and potential applications, Small 7 (11) (2011) 1504–1520.
[5] P. Greil, Perspectives of nano-carbon based engineering materials, Adv. Eng. Mater. 17 (2) (2015) 124–137.
[6] W. Lu, M. Zu, J.H. Byun, B.S. Kim, T.W. Chou, State of the art of carbon nanotube fibers: opportunities and challenges, Adv. Mater. 24 (14) (2012) 1805–1833.
[7] A.M. Beese, X. Wei, S. Sarkar, R. Ramachandramoorthy, M.R. Roenbeck, A. Moravsky, et al., Key factors limiting carbon nanotube yarn strength: exploring processing-structure-property relationships, ACS Nano 8 (11) (2014) 11454–11466.
[8] J.J. Vilatela, J.A. Elliott, A.H. Windle, A model for the strength of yarn-like carbon nanotube fibers, ACS Nano 5 (3) (2011) 1921–1927.
[9] L. Zhu, J. Wang, F. Ding, The great reduction of a carbon nanotube's mechanical performance by a few topological defects, ACS Nano 10 (6) (2016) 6410–6415.
[10] R.J. Headrick, D.E. Tsentalovich, J. Berdegue, E.A. Bengio, L. Liberman, O. Kleinerman, et al., Structure-property relations in carbon nanotube fibers by downscaling solution processing, Adv. Mater. 30 (9) (2018) 1704482.
[11] W. Xu, Y. Chen, H. Zhan, J.N. Wang, High-strength carbon nanotube film from improving alignment and densification, Nano Lett. 16 (2) (2016) 946–952.
[12] A.A. Kuznetsov, A.F. Fonseca, R.H. Baughman, A.A. Zakhidov, Structural model for dry-drawing of sheets and yarns from carbon nanotube forests, ACS Nano 5 (2) (2011) 985–993.
[13] E.R. Meshot, D.W. Zwissler, N. Bui, T.R. Kuykendall, C. Wang, A. Hexemer, et al., Quantifying the hierarchical order in self-aligned carbon nanotubes from atomic to micrometer scale, ACS Nano 11 (6) (2017) 5405–5416.
[14] Q. Li, Y.L. Kang, W. Qiu, Y.L. Li, G.Y. Huang, J.G. Guo, et al., Deformation mechanisms of carbon nanotube fibres under tensile loading by in situ Raman spectroscopy analysis, Nanotechnology 22 (22) (2011) 225704.
[15] W.L. Deng, W. Qiu, Q. Li, Y.L. Kang, J.G. Guo, Y.L. Li, et al., Multi-scale experiments and interfacial mechanical modeling of carbon nanotube fiber, Exp. Mech. 54 (1) (2013) 3–10.
[16] J.Y. Zhou, G.Z. Sun, Z.Y. Zhan, J.N. An, L.X. Zheng, E.Q. Xie, Probing structure and strain transfer in dry-spun carbon nanotube fibers by depth-profiled Raman spectroscopy, Appl. Phys. Lett. 103 (3) (2013) 031912.
[17] Y.N. Zhang, L.X. Zheng, G.Z. Sun, Z.Y. Zhan, K. Liao, Failure mechanisms of carbon nanotube fibers under different strain rates, Carbon 50 (8) (2012) 2887–2893.
[18] G.Z. Sun, L.X. Zheng, J.Y. Zhou, Y.N. Zhang, Z.Y. Zhan, J.H.L. Pang, Load-transfer efficiency and mechanical reliability of carbon nanotube fibers under low strain rates, Int. J. Plast. 40 (2013) 56–64.
[19] G.Z. Sun, J.H.L. Pang, J.Y. Zhou, Y.N. Zhang, Z.Y. Zhan, L.X. Zheng, A modified weibull model for tensile strength distribution of carbon nanotube fibers with strain rate and size effects, Appl. Phys. Lett. 101 (13) (2012) 131905.
[20] F.A. Hill, T.F. Havel, A.J. Hart, C. Livermore, Enhancing the tensile properties of continuous millimeter-scale carbon nanotube fibers by densification, ACS Appl. Mater. Interfaces 5 (15) (2013) 7198–7207.
[21] K. Liu, Y. Sun, X. Lin, R. Zhou, J. Wang, S. Fan, et al., Scratch-resistant, highly conductive, and high-strength carbon nanotube-based composite yarns, ACS Nano 4 (10) (2010) 5827–5834.
[22] S. Ryu, Y. Lee, J.W. Hwang, S. Hong, C. Kim, T.G. Park, et al., High-strength carbon nanotube fibers fabricated by infiltration and curing of mussel-inspired catecholamine polymer, Adv. Mater. 23 (17) (2011) 1971–1975.
[23] X.H. Zhong, Y.L. Li, Y.K. Liu, X.H. Qiao, Y. Feng, J. Liang, et al., Continuous multilayered carbon nanotube yarns, Adv. Mater. 22 (6) (2010) 692–696.
[24] L. Ci, N. Punbusayakul, J.Q. Wei, R. Vajtai, S. Talapatra, P.M. Ajayan, Multifunctional macroarchitectures of double-walled carbon nanotube fibers, Adv. Mater. 19 (13) (2007) 1719–1723.
[25] X.B. Zhang, K.L. Jiang, C. Teng, P. Liu, L. Zhang, J. Kong, et al., Spinning and processing continuous yarns from 4-inch wafer scale super-aligned carbon nanotube arrays, Adv. Mater. 18 (12) (2006) 1505–1510.
[26] X.F. Zhang, Q.W. Li, T.G. Holesinger, P.N. Arendt, J.Y. Huang, P.D. Kirven, et al., Ultrastrong, stiff, and lightweight carbon-nanotube fibers, Adv. Mater. 19 (23) (2007) 4198–4201.
[27] A. Ghemes, Y. Minami, J. Muramatsu, M. Okada, H. Mimura, Y. Inoue, Fabrication and mechanical properties of carbon nanotube yarns spun from ultra-long multi-walled carbon nanotube arrays, Carbon 50 (12) (2012) 4579–4587.
[28] M. Miao, Electrical conductivity of pure carbon nanotube yarns, Carbon 49 (12) (2011) 3755–3761.
[29] C.D. Tran, W. Humphries, S.M. Smith, C. Huynh, S. Lucas, Improving the tensile strength of carbon nanotube spun yarns using a modified spinning process, Carbon 47 (11) (2009) 2662–2670.
[30] M. Zu, Q. Li, Y. Zhu, M. Dey, G. Wang, W. Lu, et al., The effective interfacial shear strength of carbon nanotube fibers in an epoxy matrix characterized by a microdroplet test, Carbon 50 (3) (2012) 1271–1279.
[31] Y. Nakayama, Synthesis, nano processing, and yarn application of carbon nanotubes, Jpn. J. Appl. Phys. 47 (10) (2008) 8149–8156.
[32] C. Jayasinghe, S. Chakrabarti, M.J. Schulz, V. Shanov, Spinning yarn from long carbon nanotube arrays, J. Mater. Res. 26 (05) (2011) 645–651.
[33] S. Zhang, L. Zhu, M.L. Minus, H.G. Chae, S. Jagannathan, C.-P. Wong, et al., Solid-state spun fibers and yarns from 1-mm long carbon nanotube forests synthesized by water-assisted chemical vapor deposition, J. Mater. Sci. 43 (13) (2008) 4356–4362.
[34] K. Liu, F. Zhu, L. Liu, Y. Sun, S. Fan, K. Jiang, Fabrication and processing of high-strength densely packed carbon nanotube yarns without solution processes, Nanoscale 4 (11) (2012) 3389–3393.
[35] G. Xu, J. Zhao, S. Li, X. Zhang, Z. Yong, Q. Li, Continuous electrodeposition for lightweight, highly conducting and strong carbon nanotube-copper composite fibers, Nanoscale 3 (10) (2011) 4215–4219.
[36] K. Liu, Y. Sun, R. Zhou, H. Zhu, J. Wang, L. Liu, et al., Carbon nanotube yarns with high tensile strength made by a twisting and shrinking method, Nanotechnology 21 (4) (2010) 045708.
[37] J.N. Wang, X.G. Luo, T. Wu, Y. Chen, High-strength carbon nanotube fibre-like ribbon with high ductility and high electrical conductivity, Nat. Commun. 5 (2014) 3848.
[38] X.H. Zhong, R. Wang, Y.Y. Wen, Effective reinforcement of electrical conductivity and strength of carbon nanotube fibers by silver-paste-liquid infiltration processing, Phys. Chem. Chem. Phys. 15 (11) (2013) 3861–3865.
[39] K.R. Atkinson, S.C. Hawkins, C. Huynh, C. Skourtis, J. Dai, M. Zhang, et al., Multifunctional carbon nanotube yarns and transparent sheets: fabrication, properties, and applications, Physica B 394 (2) (2007) 339–343.
[40] N. Behabtu, C.C. Young, D.E. Tsentalovich, O. Kleinerman, X. Wang, A.W. Ma, et al., Strong, light, multifunctional fibers of carbon nanotubes with ultrahigh conductivity, Science 339 (6116) (2013) 182–186.
[41] L.M. Ericson, H. Fan, H. Peng, V.A. Davis, W. Zhou, J. Sulpizio, et al., Macroscopic, neat, single-walled carbon nanotube fibers, Science 305 (5689) (2004) 1447–1450.

[42] K. Koziol, J. Vilatela, A. Moisala, M. Motta, P. Cunniff, M. Sennett, et al., High-performance carbon nanotube fiber, Science 318 (5858) (2007) 1892–1895.
[43] Y.L. Li, I.A. Kinloch, A.H. Windle, Direct spinning of carbon nanotube fibers from chemical vapor deposition synthesis, Science 304 (5668) (2004) 276–278.
[44] B. Vigolo, Macroscopic fibers and ribbons of oriented carbon nanotubes, Science 290 (5495) (2000) 1331–1334.
[45] M. Zhang, K.R. Atkinson, R.H. Baughman, Multifunctional carbon nanotube yarns by downsizing an ancient technology, Science 306 (5700) (2004) 1358–1361.
[46] H.W. Zhu, C.L. Xu, D.H. Wu, B.Q. Wei, R. Vajtai, P.M. Ajayan, Direct synthesis of long single-walled carbon nanotube strands, Science 296 (5569) (2002) 884–886.
[47] L.K. Randeniya, A. Bendavid, P.J. Martin, C.D. Tran, Composite yarns of multiwalled carbon nanotubes with metallic electrical conductivity, Small 6 (16) (2010) 1806–1811.
[48] S. Zhang, K.K. Koziol, I.A. Kinloch, A.H. Windle, Macroscopic fibers of well-aligned carbon nanotubes by wet spinning, Small 4 (8) (2008) 1217–1222.
[49] X. Zhang, Q. Li, Y. Tu, Y. Li, J.Y. Coulter, L. Zheng, et al., Strong carbon-nanotube fibers spun from long carbon-nanotube arrays, Small 3 (2) (2007) 244–248.
[50] L. Zheng, G. Sun, Z. Zhan, Tuning array morphology for high-strength carbon-nanotube fibers, Small 6 (1) (2010) 132–137.
[51] H.G. Chae, B.A. Newcomb, P.V. Gulgunje, Y. Liu, K.K. Gupta, M.G. Kamath, et al., High strength and high modulus carbon fibers, Carbon 93 (2015) 81–87.
[52] B.A. Newcomb, Processing, structure, and properties of carbon fibers, Compos. Part A 91 (2016) 262–282.
[53] Q. Li, J.S. Wang, Y.L. Kang, Y.L. Li, Q.H. Qin, Z.L. Wang, et al., Multi-scale study of the strength and toughness of carbon nanotube fiber materials, Mater. Sci. Eng., A 549 (2012) 118–122.
[54] Y. Fan, B.R. Goldsmith, P.G. Collins, Identifying and counting point defects in carbon nanotubes, Nat. Mater. 4 (12) (2005) 906–911.
[55] Y. Fan, M. Burghard, K. Kern, Chemical defect decoration of carbon nanotubes, Adv. Mater. 14 (2) (2002) 130–133.
[56] A. Felten, X. Gillon, M. Gulas, J.J. Pireaux, X. Ke, G. Van Tendeloo, et al., Measuring point defect density in individual carbon nanotubes using polarization-dependent X-ray microscopy, ACS Nano 4 (8) (2010) 4431–4436.
[57] P.G. Collins, Defects and Disorder in Carbon Nanotubes, Oxford Handbook of Nanoscience and Technology: Volume 2: Materials: Structures, Properties and Characterization Techniques, vol. 2, 2010, p. 31.
[58] B.R. Goldsmith, J.G. Coroneus, V.R. Khalap, A.A. Kane, G.A. Weiss, P.G. Collins, Conductance-controlled point functionalization of single-walled carbon nanotubes, Science 315 (5808) (2007) 77–81.
[59] W. Wang, S. Dai, X. Li, J. Yang, D.J. Srolovitz, Q. Zheng, Measurement of the cleavage energy of graphite, Nat. Commun. 6 (2015) 7853.
[60] S. Cranford, H.M. Yao, C. Ortiz, M.J. Buehler, A single degree of freedom 'lollipop' model for carbon nanotube bundle formation, J. Mech. Phys. Solid. 58 (3) (2010) 409–427.
[61] M. Zhang, S. Fang, A.A. Zakhidov, S.B. Lee, A.E. Aliev, C.D. Williams, et al., Strong, transparent, multifunctional, carbon nanotube sheets, Science 309 (5738) (2005) 1215–1219.
[62] M. Ouyang, J.L. Huang, C.L. Cheung, C.M. Lieber, Atomically resolved single-walled carbon nanotube intramolecular junctions, Science 291 (5501) (2001) 97–100.
[63] J.F. Colomer, L. Henrard, G. Van Tendeloo, A. Lucas, P. Lambin, Study of the packing of double-walled carbon nanotubes into bundles by transmission electron microscopy and electron diffraction, J. Mater. Chem. 14 (4) (2004) 603–606.
[64] M.F. Yu, O. Lourie, M.J. Dyer, K. Moloni, T.F. Kelly, R.S. Ruoff, Strength and breaking mechanism of multiwalled carbon nanotubes under tensile load, Science 287 (5453) (2000) 637–640.
[65] A.H. Barber, R. Andrews, L.S. Schadler, H.D. Wagner, On the tensile strength distribution of multiwalled carbon nanotubes, Appl. Phys. Lett. 87 (20) (2005) 203106.
[66] A.H. Barber, I. Kaplan-Ashiri, S.R. Cohen, R. Tenne, H.D. Wagner, Stochastic strength of nanotubes: an appraisal of available data, Compos. Sci. Technol. 65 (15–16) (2005) 2380–2384.
[67] M. Yang, V. Koutsos, M. Zaiser, Size effect in the tensile fracture of single-walled carbon nanotubes with defects, Nanotechnology 18 (15) (2007) 155708.
[68] Z.Q. Zhang, B. Liu, Y.W. Zhang, K.C. Hwang, H.J. Gao, Ultra-strong collagen-mimic carbon nanotube bundles, Carbon 77 (2014) 1040–1053.
[69] X. Wei, M. Naraghi, H.D. Espinosa, Optimal length scales emerging from shear load transfer in natural materials: application to carbon-based nanocomposite design, ACS Nano 6 (3) (2012) 2333–2344.
[70] X.L. Gao, K. Li, A shear-lag model for carbon nanotube-reinforced polymer composites, Int. J. Solid Struct. 42 (5–6) (2005) 1649–1667.
[71] Q.Q. Rong, J.S. Wang, Y.L. Kang, Y.L. Li, Q.H. Qin, A damage mechanics model for twisted carbon nanotube fibers, Acta Mech. Solida Sin. 25 (4) (2012) 342–347.
[72] X.L. Wei, Q. Chen, L.M. Peng, R.L. Cui, Y. Li, Tensile loading of double-walled and triple-walled carbon nanotubes and their mechanical properties, J. Phys. Chem. C 113 (39) (2009) 17002–17005.
[73] W. Ding, L. Calabri, K.M. Kohlhaas, X. Chen, D.A. Dikin, R.S. Ruoff, Modulus, fracture strength, and brittle vs. plastic response of the outer shell of arc-grown multi-walled carbon nanotubes, Exp. Mech. 47 (1) (2006) 25–36.
[74] B. Peng, M. Locascio, P. Zapol, S. Li, S.L. Mielke, G.C. Schatz, et al., Measurements of near-ultimate strength for multiwalled carbon nanotubes and irradiation-induced crosslinking improvements, Nat. Nanotechnol. 3 (10) (2008) 626–631.
[75] J.M. Carlsson, Curvature and chirality dependence of the properties of point defects in nanotubes, Phys. Status Solidi B 243 (13) (2006) 3452–3457.
[76] M.F. Yu, B.S. Files, S. Arepalli, R.S. Ruoff, Tensile loading of ropes of single wall carbon nanotubes and their mechanical properties, Phys. Rev. Lett. 84 (24) (2000) 5552–5555.
[77] W. Weibull, A Statistical Theory of the Strength of Materials, Ingeniors Vetenskaps Akademien, 1939.
[78] T. Filleter, R. Bernal, S. Li, H.D. Espinosa, Ultrahigh strength and stiffness in cross-linked hierarchical carbon nanotube bundles, Adv. Mater. 23 (25) (2011) 2855–2860.
[79] H.E. Daniels, The statistical theory of the strength of bundles of threads, Int. Proc. R. Soc. Lond. A 183 (995) (1945) 0405–0435.
[80] X. Wei, T. Filleter, H.D. Espinosa, Statistical shear lag model - unraveling the size effect in hierarchical composites, Acta Biomater. 18 (2015) 206–212.
[81] Z.Q. Zhang, B. Liu, Y. Huang, K.C. Hwang, H. Gao, Mechanical properties of unidirectional nanocomposites with non-uniformly or randomly staggered platelet distribution, J. Mech. Phys. Solid. 58 (10) (2010) 1646–1660.
[82] M. Motta, A. Moisala, I.A. Kinloch, A.H. Windle, High performance fibres from 'dog bone' carbon nanotubes, Adv. Mater. 19 (21) (2007) 3721–3726.
[83] M.F. Yu, B.I. Yakobson, R.S. Ruoff, Controlled sliding and pullout of nested shells in individual multiwalled carbon nanotubes, J. Phys. Chem. B 104 (37) (2000) 8764–8767.
[84] D.E. Soule, C.W. Nezbeda, Direct basal-plane shear in single-crystal graphite, J. Appl. Phys. 39 (11) (1968) 5122–5139.
[85] Z. Liu, J. Yang, F. Grey, J.Z. Liu, Y. Liu, Y. Wang, et al., Observation of microscale super lubricity in graphite, Phys. Rev. Lett. 108 (20) (2012) 205503.
[86] Z. Liu, S.M. Zhang, J.R. Yang, J.Z. Liu, Y.L. Yang, Q.S. Zheng, Interlayer shear strength of single crystalline graphite, Acta Mech. Sin. 28 (4) (2012) 978–982.
[87] H. Muramatsu, Y.A. Kim, T. Hayashi, M. Endo, A. Yonemoto, H. Arikai, et al., Fluorination of double-walled carbon nanotubes, Chem. Commun. (15) (2005) 2002–2004.
[88] S.H. Kim, C.S. Haines, N. Li, K.J. Kim, T.J. Mun, C. Choi, et al., Harvesting electrical energy from carbon nanotube yarn twist, Science 357 (6353) (2017) 773–778.
[89] I.Y. Stein, D.J. Lewis, B.L. Wardle, Aligned carbon nanotube array stiffness from stochastic three-dimensional morphology, Nanoscale 7 (46) (2015) 19426–19431.
[90] N.J. Ginga, W. Chen, S.K. Sitaraman, Waviness reduces effective modulus of carbon nanotube forests by several orders of magnitude, Carbon 66 (2014) 57–66.
[91] C.Y. Li, T.W. Chou, Failure of carbon nanotube/polymer composites and the effect of nanotube waviness, Compos. Part A 40 (10) (2009) 1580–1586.
[92] J. Lee, I.Y. Stein, M.E. Devoe, D.J. Lewis, N. Lachman, S.S. Kessler, et al., Impact of carbon nanotube length on electron transport in aligned carbon nanotube networks, Appl. Phys. Lett. 106 (5) (2015) 053110.
[93] F. Liu, P.M. Ming, J. Li, Ab initio calculation of ideal strength and phonon instability of graphene under tension, Phys. Rev. B 76 (6) (2007) 064120.
[94] R. Zhang, Y. Zhang, Q. Zhang, H. Xie, W. Qian, F. Wei, Growth of half-meter long carbon nanotubes based on Schulz-Flory distribution, ACS Nano 7 (7) (2013) 6156–6161.
[95] Y. Bai, R. Zhang, X. Ye, Z. Zhu, H. Xie, B. Shen, et al., Carbon nanotube bundles with tensile strength over 80 GPa, Nat. Nanotechnol. (2018). https://doi.org/10.1038/s41565-018-0141-z.
[96] P. Morgan, Carbon Fibers and Their Composites, CRC Press, 2005.